Microchemical Journal 167 (2021) 106304

Contents lists available at ScienceDirect

Microchemical Journal

journal homepage: www.elsevier.com/locate/microc

Advances in characterization of colourful residues unearthed in Persepolis West craft zone using microscopic and spectroscopic techniques

Maria Letizia Amadori [a,*], Manuela Vagnini [b], Riccardo Vivani [c], Chiara Anselmi [d], Alireza Askari Chaverdi [e], Pierfrancesco Callieri [f], Emad Matin [f], Valeria Mengacci [a]

[a] Department of Pure and Applied Sciences, University of Urbino, p.za Rinascimento 6, 61029 Urbino, Italy
[b] Diagnostic Laboratory for Cultural Heritage, piazza Campello 2, 06049 Spoleto, Italy
[c] Farmaceutical Sciences Department, University of Perugia, via del Liceo 1, 06123 Perugia, Italy
[d] Institute of Research on Terrestrial Ecosystems of National Research Council, via G. Marconi 2, 05010 Porano, Italy
[e] Department of History and Archaeology, College of Literature and Humanities, Shiraz University (CISSC), Eram Square, 71944 Shiraz, Iran
[f] Department of Cultural Heritage, University of Bologna, via degli Ariani 1, 48121 Ravenna, Italy

ARTICLE INFO

Keywords:
Colourful residues
Metal scrap
Optical and electronic microscopy
X-Ray diffraction
Infrared spectroscopy
Raman spectroscopy

ABSTRACT

The microstructure and chemical composition of blue and green pellets, coloured lump pigments and a metal scrap excavated in Persepolis West (Fars, Iran), by the *Iranian-Italian Joint Archaeological Mission in Fars* in 2008–09, were investigated to clarify their origin and production techniques.

The Persepolis West urban area has its eastern limit about five hundred meters away from the Persepolis Terrace and extends for about 1 km in a westward direction. Due to the presence in this area of various kilns and other remains, the existence of a craft zone connected with the construction of imperial and élite buildings in Persepolis was proposed.

The colourful residues were submitted to integrated investigations using portable X-ray fluorescence spectrometry, digital and polarized light microscopy, scanning electron microscopy with energy dispersive X-ray spectroscopy, X-ray diffraction, ATR-FTIR and Raman spectroscopy.

The integrated analyses allowed to identify azurite, malachite, Egyptian blue, glauconite, yellow and red ochre with hematite, magnetite and goethite. Proteinaceous material was detected only in one red lump. These pigments are in accordance with the palette used to paint the palaces of the Persepolis Terrace, thus supporting the hypothesis that in Persepolis West craft zone, there was a laboratory for production of pigments.

The microscopic features of the lumps and their peculiar shape confirmed a local manufacturing process. Moreover, the diopside presence related to the Egyptian blue production, as well as the discovery of a bronze scrap with a crust of Egyptian blue also suggested that this pigment was manufactured locally.

1. Introduction

Persepolis (Greek word for Old Persian Pārsa) is located in the Fars Province, southern Iran, about 57 km northeast of the city of Shiraz. The Persepolis Terrace (Fig. S1), an artificial platform of 125,000 m^2, houses the most celebrated buildings of the Achaemenid period [1,2]. The construction work of the Terrace started under the reign of the Achaemenid emperor Darius I (c. 518 BCE) and since then, several royal buildings have been built on this platform and its vicinity.

The Persepolis area, besides the royal sector centred on the Terrace, comprised various zones of the urban settlement with different functions, known from the written sources. Some of them belonged to the daily life of the settlement, such as Persepolis West. The eastern limit of Persepolis West urban area is located approximately 500 m from the foot of the Persepolis Terrace and this area extends approximately 1 km in a westward direction.

In 2008 and 2009, the *Iranian-Italian Joint Archaeological Mission in Fars* carried out a series of investigations in Persepolis West and surroundings and eleven trenches were excavated (Areas A-E, Trenches 1–11, Fig. S2) following the results of geophysical surveys [3–7]. The latter, carried out between the Persepolis Terrace and Persepolis West, showed a regular grid of linear anomalies, which the excavations showed to be to ditches dug into the ground. This explains that the regular network belonged to the water channels used to irrigate a green

* Corresponding author.

https://doi.org/10.1016/j.microc.2021.106304
Received 8 January 2021; Received in revised form 8 April 2021; Accepted 13 April 2021
Available online 20 April 2021

area – possibly a garden – located between the Persepolis Terrace and West Persepolis. The stretch of wall uncovered during the excavation of the same mission at one of the limits of the grid is therefore likely to represent a garden enclosure (Trench 3, Fig. S2). The location of this green area, at the foot of the Persepolis Terrace, also suggests that it formed a garden belt between the royal area and the everyday settlement. However, the exact limits of the garden and the royal area have not yet been defined [3,4]. Farther from the enclosed garden to the West, the discovery of various kilns suggested the existence of a craft production zone in Persepolis West [5–7]. One of the kilns was excavated by the joint mission [7] (Trench 4, Fig. S2).

Manufacturing objects made of different materials like metal, glass, stone, ceramic, shell and gypsum were found during these excavations. The finds also included objects such as decorative stone architectural elements, sculptural eye beads and glazed bricks [5–7]. Various colourful residues such as blue pellets, raw pigment lumps and metal scrap were discovered too (Table 1). The aforementioned finds were supposed to be related to the production of materials such as glazed bricks, plasters, moulded objects and especially pigments for the decorations of stone architectural elements.

As archaeological and written sources demonstrate, numerous craftsmen from different regions of the Empire were involved in the construction of the royal buildings, also in Persepolis [8]. Achaemenid buildings were colourful: stone reliefs were painted with various pigments and glazed bricks were used to decorate these monuments. Therefore a number of craftsmen certainly worked on pigments and painting. The activity of painters has also been recorded in the archives of Persepolis [9].

Integrated investigations were therefore carried out in order to prove that the colourful residues are strictly connected with the local artisan activity. Particular attention was given to clarify both their origin and the production technologies and – in terms of function – the possible link with the pigments used in the royal and élite buildings decoration of Persepolis Terrace.

The results of these investigations satisfied most of the above-mentioned questions. First of all, the composition of the raw pigments is compatible with that of the pigments found in Persepolis area [10–15] confirming that the craft zone served also to prepare painting materials. In addition, the Egyptian blue pigment – of which there are various testimonies in the buildings of Persepolis – was most likely produced locally in this craft area and not only imported as Matson supposed [16].

1.1. Previous studies

Coloured residues and raw pigments were found in several archaeological contexts over an extended period and different areas. These materials have usually been mentioned as pellets, lumps and sticks when they are smaller in size while considered ingots or cakes when larger.

Similar materials have been found also in Fars Province in the context of Achaemenid sites as attested by several scholars. Egyptian Blue encrustation was recovered in a potsherd in the site of Qaleh Kali [17,18]. In the Shawur Palace at Susa (Khuzestan Province), one of the administrative capitals of the Achaemenid Empire, the use of pigments is documented both for the rare Achaemenid figurative wall paintings and in pottery fragments [15,19]. Large lumps and heavy coatings of pigments were found in pottery bowls and potsherds during the excavation in the southwestern corner of the Persepolis Terrace wall [12,14]. The investigations carried out by Stodulski et al. [13] on these materials detected hematite, cinnabar, Egyptian blue, malachite, azurite. Near the Apadana (the Audience Hall), the most significant structure of the Persepolis Terrace, green, red and blue lumps were found [12,14]. Egyptian blue was detected in potsherd encrustations found in Apadana [11]. Other similar materials were discovered in the Treasury, including pigments covered stones and a basalt grinding bowl [10,14]. From the so-called Harem, a blue powdered bowl, a large number of Egyptian blue objects and glass paste pieces were unearthed [14,18]. Egyptian Blue

Table 1
Samples description, provenance and investigations.

Sample	ID Code	Trench	US	Typology	Colour	Investigations
PERS1	IR-PW-01300	7	IR-PW-Tr7-004 Area C	Lump	blue	ED-XRF, DM, PLM, SEM/EDX, XRD
PERS1a	IR-PW-01017	6	IR-PW-Tr6-031 Area B	Lump	Red	ED-XRF, DM, SEM/EDX, RAMAN, ATR/FTIR
PERS1b	IR-PW-00113a	6	IR-PW-Tr6-031 Area B	Lump	Red	ED-XRF, DM, SEM/EDX, RAMAN, ATR/FTIR
PERS1c	IR-PW-00113b	6	IR-PW-Tr6-031 Area B	Lump	Yellow	ED-XRF, DM, SEM/EDX, RAMAN, ATR/FTIR, XRD
PERS2	IR-PW-01301	7	IR-PW-Tr7-006 Area C	Lump	Yellow	ED-XRF, DM, SEM/EDX, RAMAN, ATR/FTIR, XRD
PERS2a	IR-PW-01301	7	IR-PW-Tr7-006 Area C	Lump	Yellow	ED-XRF, DM, SEM/EDX, RAMAN, ATR/FTIR
PERS3	IR-PW-01302	9	IR-PW-Tr9-002 Area D	Pellet	blue	ED-XRF, DM, PLM, SEM/EDX, ATR/FTIR, XRD
PERS3a	IR-PW-01302	9	IR-PW-Tr9-002 Area D	Pellet	Blue	ED-XRF, DM, SEM/EDX, ATR/FTIR, XRD
PERS4a	IR-PW-01303	9	IR-PW-Tr9-002 Area D	Lump	Green	ED-XRF, DM, PLM, SEM/EDX, XRD
PERS4b	IR-PW-01303	9	IR-PW-Tr9-002 Area D	Lump	Red	ED-XRF, DM, PLM, SEM/EDX, RAMAN
PERS6	IR-PW-01305	10	IR-PW-Tr10-004 Area D	Alloy	Red and green	ED-XRF, DM, PLM, SEM/EDX
PERS7a	IR-PW-0180	10	IR-PW-Tr10-013 Area D	Pellet	Blue	ED-XRF, DM, SEM/EDX, ATR/FTIR, XRD
PERS8	IR-PW-01307	10	IR-PW-Tr10-0011 Area D	Lump	Yellow	ED-XRF, DM, SEM/EDX, ATR/FTIR, XRD
PERS9	IR-PW-01308	11	IR-PW-Tr11-008 Area E	Lump	Yellow	ED-XRF, DM, PLM, SEM/EDX, RAMAN, ATR/FTIR, XRD
PERS10	IR-PW-01309	11	IR-PW-Tr11-009 Area E	Lump	Reddish	ED-XRF, DM, SEM/EDX, ATR/FTIR
PERS11	IR-PW-01310	11	IR-PW-Tr11-0014 Area E	Lump	Red	ED-XRF, DM, SEM/EDX, RAMAN, ATR/FTIR
PERS12a-b	IR-PW-01311	11	IR-PW-Tr11-0015 Area E	Lump	Red and white	ED-XRF, DM, PLM, SEM-EDX, ATR/FTIR, XRD
PERS13	IR-PW-01312	8	IR-PW-Tr8-010 Area D	Lump	Yellow	ED-XRF, DM, PLM, SEM/EDX, RAMAN, ATR/FTIR
PERS14	IR-PW-01313	8	IR-PW-Tr8-003 Area C	Pellet	Blue	ED-XRF, DM, SEM/EDX
PERS15	IR-PW-01314	8	IR-PW-Tr8-006 Area C	Pellet	Blue	ED-XRF, DM, PLM, SEM/EDX

encrustation and green pigment were found in Achaemenid pottery in Dasht-e Gohar, about 3.5 km to the north of the Persepolis Terrace [12]. We should also consider that several metallurgical remains were found in the archaeological excavations north-west of the Terrace [20] and a metal slag fragment was found by Herzfeld north of the Terrace [15].

The archaeologists assumed that the above-mentioned materials found on the Persepolis Terrace had been presumably used by the craftsmen working there. Obviously, polychromy could have been applied to different materials, such as ceramic, wood and jewellery [14]. But what is essential for the discussion at hand is that at least part of the stone reliefs and the architectural elements of Persepolis Terrace were covered with different colours [18]. The colouration of stone elements was typical of the ancient Middle East even before the Achaemenid period. The use of this method is well documented in Neo-Assyrian reliefs [21,22].

The occurrence of pigments on the stones of the Persepolis Terrace buildings was not only described by some ancient travellers, but also by early excavators who commented on the occasional presence of coloured pigments on the newly exposed surfaces. Several pigments were identified on stone building surfaces of Persepolis Terrace such as Egyptian blue, malachite, azurite, cinnabar, hematite, goethite, limonite, the rare mineral tyrolite, tenorite, and realgar/orpiment [13,23,24]. Archaeometric investigations carried out on stone materials from Naqsh-e Rostam showed traces of Egyptian blue, malachite, hematite, cinnabar and yellow ochre [12–14,25]. Coloured plasters made of hematite and cinnabar have been found in the building's floors (e.g. Treasury). Besides, some fragments of plaster with painted drawings were unearthed during the excavation in Persepolis Terrace and in other Achaemenid structures [13,16,24–26]. In some cases, green plaster has been used to cover the mud-brick walls, such as Complex A at Barzan-e Jonubi, the southern field of the Persepolis Terrace [27].

The discovery of traces of blue colour has raised the question whether Egyptian blue might had been produced in this area or the workshop was responsible only for applying the colour on the ceramic objects. Matson [16] analysed fragments of objects and proposed that Egyptian blue had been imported to Persepolis in the form of lumps or powder to be used as pigments. One of the most interesting finds from the excavations at Persepolis West is a fragment of moulded decoration representing a feathered right-wing in Egyptian blue [20]. Two knobs probably composed of Egyptian blue were unearthed in Persepolis during the excavation respectively in the drainage channels built in the foundations of the Persepolis Terrace [28] and in the aforementioned Barzan-e Jonubi [27].

Another group of architectural elements and decorations unearthed during the excavation in Persepolis West are three fragments of different coloured glazed bricks [20]. One of them is akin to the typical siliceous Achaemenid glazed bricks also used for decorating monuments of the Terrace [10,29]. The two other fragments of clayey bricks are instead similar to the materials recently discovered at the Early Achaemenid monumental gate of Tol-e Ajori, located in Bagh-e Firuzi urban area and 3.5 km far from the Terrace [30–32].

2. Experimental section

2.1. Sampling

On the basis of the results of preliminary non-invasive investigation as explained below, 21 micro-samples (Table 1; Fig. S3) were collected from various colour residues consisting of pellets (blue), lumps of pigments (green, blue, red and yellow) and metal scrap. The finds were unearthed at Persepolis West (Fig. S1) in Trenches Tr. 6 (Area B), Tr. 7 and Tr. 8 (Area C), Tr. 9 and Tr. 10 (Area D) and Tr. 11 (Area E) (Fig. S2).

Sampling was carefully carried out depending on surface characteristics and colour hue, according to the pressing requirements of conservation philosophy. In Table 1 are indicated typology, colour and the identification code of samples.

2.2. Instruments and methods

Ensuring that the investigated materials were representative was very difficult, due to their inhomogeneity, and the selection was supported by digital microscopic observation and energy-dispersive X-ray fluorescence analysis. Each colour residue was deeply observed to find out the most homogeneous areas on the basis of their colour and grainsize. The selected uniform areas of each residue were divided into four portions that were widely analysed by ED-XRF. Then sampling was carried out where the chemical composition was more homogeneous. These samples were divided into various portions required for the different micro destructive investigations after proper preparation.

2.3. Digital microscopy (DM)

Observations with digital microscope were preliminary carried out using Dino-Lite Universal USB digital microscope (AM7013MZT4, interface USB 2.0, sensor CMOS 5 Megapixel, equipped with polarizer anti-reflection and IR cut-filter >650 nm), directly connected to PC. Images were acquired with 50x and 230x magnifications.

2.4. Energy dispersive ED (ED-XRF)

Energy Dispersive X-ray fluorescence analysis was carried out using an Oxford Instrument X-Met 8000 energy dispersive handheld spectrometer, with X-Flash SDD detector and 6 mm diameter spot, with a Rh target X-ray tube operating both at 8 kV, 50 μA and 40 kV, 8 μA. The first operating condition is particularly sensitive to light elements (from about Al), the second to heavier ones including Sn, Sb and Ba K-lines. The measurement time was 60 s: 44 s at 8 kV and 16 s at 40 kV. Data were processed using proper software like Artax.

2.5. Polarised light microscopy (PLM)

A small portion of pigments pellets and lumps was embedded in epoxy resin support (SeriFix resin, Struers) then carefully polished after curing of the resin with progressively finer silicon carbide cards. Some samples were carefully ground to final thickness (usually 30 μm) to be made into thin sections.

The observations on polished cross-sections and thin sections were performed using an OLYMPUS BX51 polarized light microscope equipped with fixed oculars of 10x and objectives with different magnifications (5, 10, 20, 50 and 100x), directly connected to an Olympus SC50 camera and Stream Basic software for images acquisition. The examination provides information on mineralogical compositions, size and characteristics of crystals and particles.

Observations were carried out both in reflection and transmission modes on unetched and etched surfaces. The following solvents were used for etching: hydrochloric acid (37% ref. 320331) and Iron (III) chloride (97% ref. 157740) purchased from Sigma-Aldrich (Milan, Italy). The aqueous ferric chloride solution was used at 6% w/v according to Scott [33].

2.6. Scanning electron microscopy – Energy-Dispersive X-ray spectroscopy (SEM-EDS)

An Electron scanning microscope Hitachi Tabletop TMT3030, equipped with an energy dispersive X-Ray spectrometer and dedicated software Quantax 70, was used both on samples and cross-sections without any conductive coating. The measurements were performed using 20 kV acceleration voltage with a variable working distance (from 7.3 to 11.4 mm). Operative conditions were 30KeV with an average lifetime of 40 s. Samples and cross-sections were analysed using backscattered electron (BSE) mode.

2.7. Powder X-ray diffraction (XRD)

X-ray diffraction data were collected directly on the sample's surface in theta-theta reflection geometry with the CuKα radiation (λ = 1.54056 Å) on PANalytical X'PERT PRO diffractometer, PW3050 goniometer equipped with an X'Celerator fast detector. The Long Fine Focus tube operated at 40KV, 40 mA. Data were collected using a step size of 0.017° and a count time of 10 s per step. Positions of diffraction maxima for phase identification were determined by the second derivative method and the results processed with the PANalytical X'Pert Highscore search – match program with the help of the ICDD-PDF database.

2.8. Attenuated total reflectance fourier transform infrared spectroscopy (ATR/FTIR)

The portable infrared spectrophotometer ALPHA (Bruker Optik GmbH), equipped with a Globar IR source, an interferometer (Rock-Solid)™, insensitive to external vibrations and able to work in any spatial orientation), a DLaTGS room temperature detector and an ATR accessory with a diamond crystal was used. The IR spectra were acquired in the spectral range 4000–375 cm^{-1} with a spectral resolution of 4 cm^{-1} and 128 interferograms. The sample to be analysed does not require preparation and was placed directly onto the sample probe.

2.9. Portable Raman spectroscopy

The BRAVO spectrometer uses a new-patented technology called SSE™ (Sequentially Shifted Excitation, patent number US8570507B1) to mitigate fluorescence [34,35]. The laser is slightly wavelength shifted during the acquisition for three times, and three raw Raman spectra are recorded. A proper algorithm recognizes all the peak that shift at different laser wavelength as good Raman peaks, and other peaks, non-shifting, as fluorescence (or absorbance) peaks, removing them. Moreover, the BRAVO uses two different lasers (DuoLaser™), ranging from 700 to 1100 nm, during the acquisition. The use of the second laser is not intended as in standard commercial handheld or portable Raman spectrometer as a tool to try to mitigate the fluorescence, but as a way to collect Raman spectra up to 3200 cm^{-1} and hence to access the CH stretching region also. The first laser is dedicated to the acquisition of the Raman spectra in the first range (called fingerprint region), the second one in the second range (called CHregion). The BRAVO acquired spectrum is finally a Raman spectrum free from fluorescence on a whole spectral range from 3200 cm^{-1} to 300 cm^{-1}. The applied laser power is always<100 mW for both lasers. Using the BRAVO two lasers ranging from 700 to 1100 nm, the sensitivity to inorganic green and blue is really reduced if compared to the use of a 532 nm laser. The spectral information from the enhanced spectral range is useful for identification, for example, of resins and waxes. The spectra were acquired with acquisition time ranging from 500 ms to 2 s and accumulation ranging from 5 to 100. For all the measurements, OPUS™ software (Version 7.7) has been used to select the appropriate acquisition parameters.

3. Results

Firstly, attentive observations of the colour residues (Table 1; Fig. S3) and metal scrap were carried out by using a digital microscope to distinguish surface texture and hues. As the basis for the following sampling and micro destructive investigations, energy-dispersive X-ray fluorescence analysis was carried out on the finds to provide preliminary information concerning the constituting elements.

Combining the results acquired by integrated techniques (PLM, SEM-EDS, XRD, ATR-FTIR, Raman) it was possible to fully characterize the samples.

The discussion of the results is reported by the colour samples for easy reading. In the case of colour mixtures, the samples were classified on the base of the predominant hue. In Tables 2a–2d, the results obtained by the different investigations on the cross-sections, fragments and powders are summarized.

Table 2a
Composition of blue and green samples by integrated investigations.

Sample	ED-XRF	SEM/EDX	Raman	ATR/FTIR	XRD
PERS1	Cu, Si, Al, Ca, Fe, K	Cu, Si, (Al, K, Fe, Mg, Na)	/	/	Quartz, azurite, calcite
PERS4a	Cu, Ca, Si, Fe, K, Ti (Cl)	Cu, Si, (Al, K, Fe, Mg, Ti, Cr, Ca)	/	/	Malachite, quartz, potassium-magnesium silicate, kaolinite glauconite
PERS3	Cu, Ca, Si, Fe, Cl	Si, Ca, Cu (Al, Mg, Cl, Fe)	/	Calcium carbonate, kaolinite, phyllosilicates	Cuprorivaite, quartz, calcite
PERS3a	Cu, Ca, Si, Fe, K, (S)	Si, Cu, Ca Silicates particles: Si, Ca, Al, Fe, Mg, K, (Na) Fe-based particles: Fe, Si, Ca, Al, Cr, Mg, K, (Na)	/	Silicates calcium carbonate	Cuprorivaite, quartz, calcite, pyroxene
PERS7a	Cu, Ca, Si, Fe, K, Sr, Ti	Si, Cu, Ca (Mg, Fe, Al)	/	Egyptian Blue calcium carbonate	Quartz, cuprorivaite, diopside, calcite
PERS14	Cu, Ca, Si, Fe, (Sr)	Si, Ca, Cu (Na, Al, Mg, Ti, Cl) Fe-based particles: Si, Fe, Cr, Ca, Al, Mg HgS particles	/	/	/
PERS15	Cu, Ca, Si, Fe, (Sr)	Si, Ca, Cu, (Al, Fe, K, Mg, S, Cl) Fe-Cr particles	/	/	/

3.1. Blue and green pellets

3.1.1. Azurite and malachite

The samples PERS1 and PERS4a (Table 1), respectively pale blue (Fig. 1a) and green (Fig. 1c), are both rounded in shape (Fig. S3).

ED-XRF analysis carried out within the bulk composition of both the samples evidenced the ubiquitous presence of Cu and Si (Table 2a) with few amounts of Al, Fe, K, Ti and Cr.

High birefringence microcrystals attributable to azurite were observed in sample PERS1 by polarized light microscopy (PLM). The azurite crystals are very fine-grained (particle sizes < 100μ) with blue colour and weak pleochroism (Fig. 1b). Mono and polycrystalline quartz having a shape varying from angular to sub-angular and few iron oxides are also present. A carbonate deposit with a thickness not exceeding 200 μm covered the external surface of the sample.

SEM-EDS investigations of sample PERS1 (Table 2a, S1; Fig. S4a-c) allowed to identify a Cu-based matrix, fibrous fine-grained Si-Al-K-based forms and Si-based crystals varying in size. Fe-rich oxides particles were

Table 2b
Composition of yellow samples by integrated investigations.

Sample	ED-XRF	SEM/EDX	Raman	ATR/FTIR	XRD
PERS1c	Fe, Ca, K, Si, Ti	Fe, Si, Al, K, (Mg, Ti, Ca)	Yellow ochre, calcite	Calcium carbonate, kaolinite, goethite, hematite	Quartz, goethite, kaolinite
PERS2	Ca, Fe, Si, Sr, (K)	Si, Ca, (Al, Mg, Fe, C, P) Particles (Si, Ca, Al K, Fe, Mg, Na, Ti)	Calcite	Calcium carbonate, quartz	Calcite, quartz
PERS2a	Ca, Fe, Sr, K	Ca, Si, Fe, Al, (Mg, K, Ti) Particles (Ba, Ca, S, Si, Al, Fe, K, Mg, Ti)	Calcite	Calcium carbonate, kaolinite, hematite	/
PERS8	Ca, Fe, Si, K, Al Ti, (Sr)	Ca, Si, Fe, Al, K, Mg, Ti, S, Na, Mn, Zr	/	Calcium carbonate, aragonite	Calcite, quartz, dolomite, Fe-chlorite, (potassium magnesium silicate, muscovite and albite)
PERS9	Ca, Si, Fe, K, Ti Sr, (Al)	Ca, Fe, Al, K, Particles (Fe, Ca, Si, Mn, Al, Mg, K) White area (Si, Ca, Al, Fe, Mg, K, Na, Ti)	Calcite	Kaolinite, calcium carbonate, hematite	Quartz, calcite, Fe-chlorite, dolomite, muscovite, palygorskite
PERS13	Ca, Fe, Si, K, S (Ti, Sr, Al)	Ca, Si, Fe, Al, Na, Mg Particles (Fe, Si)	Magnetite, goethite	Calcium carbonate, silicates	/

Table 2c
Composition of red samples by integrated investigations.

Sample	ED-XRF	SEM/EDX	Raman	ATR/FTIR	XRD
PERS1a	Fe, Ca, Si, K, Ti, Al	Fe, Si, Al (K, Mg, Ti, Ca) White areas: Si, Fe, Al (Ti, Mg, K)	Hematite	Kaolinite, phyllosilicates	/
PERS1b	Fe, Ti, Ca, As, (K)	Fe (Si, Mg, Ca, Al, As, P)	Hematite	Hematite, phyllosilicates, organic compound	/
PERS4b	Fe, Ca, Sr	Fe, Ca, (Si, Al, Mg, K)	Red ochre calcite	/	/
PERS10	Ca, Si, Fe, K, Ti, Sr	Pinkish area: matrix: Ca, Si, (Al, Fe, Mg, K). Red compact area: Ca, (Si, Al, Fe, Mg, K) Cu-based particle (Cu, Ca, Cl, Si, Al, Fe, Mg, K)	/	Goethite, calcium carbonate, kaolinite	/
PERS11	Fe, Ca, (Si)	Fe, Si, Ca, Al, K, Mg, Cl, Ca-P particle, Ag Clast: (Fe, Al, Si, Mg) Sb-Pb particles	Hematite	Calcium carbonate, quartz, kaolinite, aragonite	/
PERS12a red area	Si, Fe, Ca, K	Fe, Si, Ca, (Al, K, Mg) Fe-based particles	/	Calcium carbonate silicates	/
PERS12b white area	Ca, Si, Fe, K, Sr, Ti, (Zr, Mn, Al)	Ca, Si, Al, Fe, K, Mg Fe-based particles	/	/	Quartz, calcium carbonate, Fe-chlorite, dolomite, muscovite, palygorskite

Table 2d
Composition of metal scrap sample by integrated investigations.

Sample		ED-XRF	SEM/EDX
PERS 6	green area	Cu, Ca, Cl, Sn, Si, S, Fe, Pb, K, Cr	(particles), Cu, Si, Ca (Al, Mg, Na, K)
	red area	Cu, Ca, Sn, Cl, Pb, Fe, Mn, Si, S, (Cr, Zn, Sr)	Cu, Sn, Si (Al, Fe, Pb, Mg, Cl)

also detected.

XRD analysis of sample PERS1 (Tables S2, 2a; Fig. 2a) identified azurite ($Cu_3(CO_3)_2{\cdot}(OH)_2$), quartz and calcite.

According to PLM observation, sample PERS4a (Fig. 1d) consists of a mixture of very fine-grained malachite microcrystals (particle sizes <125μ). In brown-green matrix clay minerals (glauconite) and rare iron oxides were observed. Malachite is recognized for its prismatic-fibrous structure, twinning, very high birefringence, dark edges, green and pale green colour. The finer particles are colourless, while high pleochroism is noticeable in the coarser one. Mono and polycrystals of quartz were observed, their grain size ranges from 4 to 250 μ.

SEM-EDS investigations of sample PERS4a (Table 2a, S1; Fig. S5a-b) allowed to identify a Cu-based matrix. Fe, Mg, Ti, Cr, Ca as impurities were detected too.

XRD spectrum of sample PERS4a showed malachite ($Cu_2CO_3{\cdot}(OH)_2$), quartz, potassium-magnesium silicate, kaolinite and glauconite were less evident (Table 2a, S2; Fig. 2b).

3.1.2. Egyptian blue

The five blue pellets (samples PERS3, PERS3a, PERS7a, PERS14, PERS15; Table 1) show variable hues and rounded shapes (Fig. S3). ED-XRF analyses evidenced the ubiquitous presence of Si, Cu and Ca throughout the bulk composition, (Table 2a) suggesting the Egyptian blue occurrence.

The blue crystals observed by DM and PLM show euhedral and tabular shapes according to the literature [36]. Samples PERS3 (Fig. 3a-b) and PERS3a (Fig. S6a) are coarser than samples PERS14 and PERS7a. Sample PERS 15 is very fine-grained (Fig. 3c-d). The cuprorivaite crystals size varies from a maximum of 500 μ, in sample PERS3, to a minimum of 50 μ in sample PERS15 (estimated average size of 250 μ). The samples are mainly composed of pleochroic cuprorivaite microcrystals

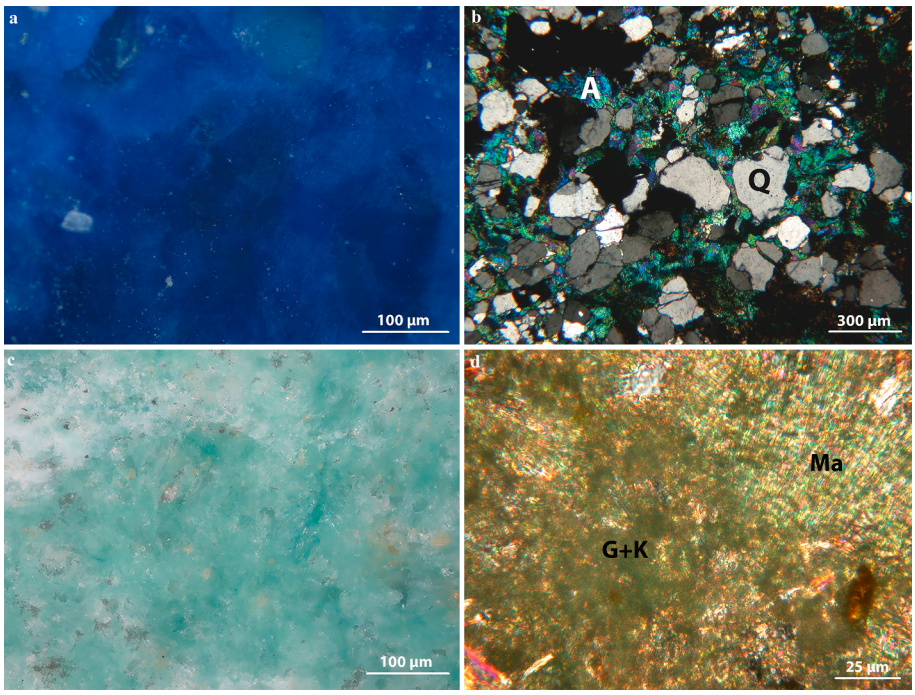

Fig. 1. Blue lump: PLM micrographs in (a) reflected light and (b) transmitted light (XPL). Green lump: PLM micrographs in (c) reflected light and (d) transmitted light (XPL).

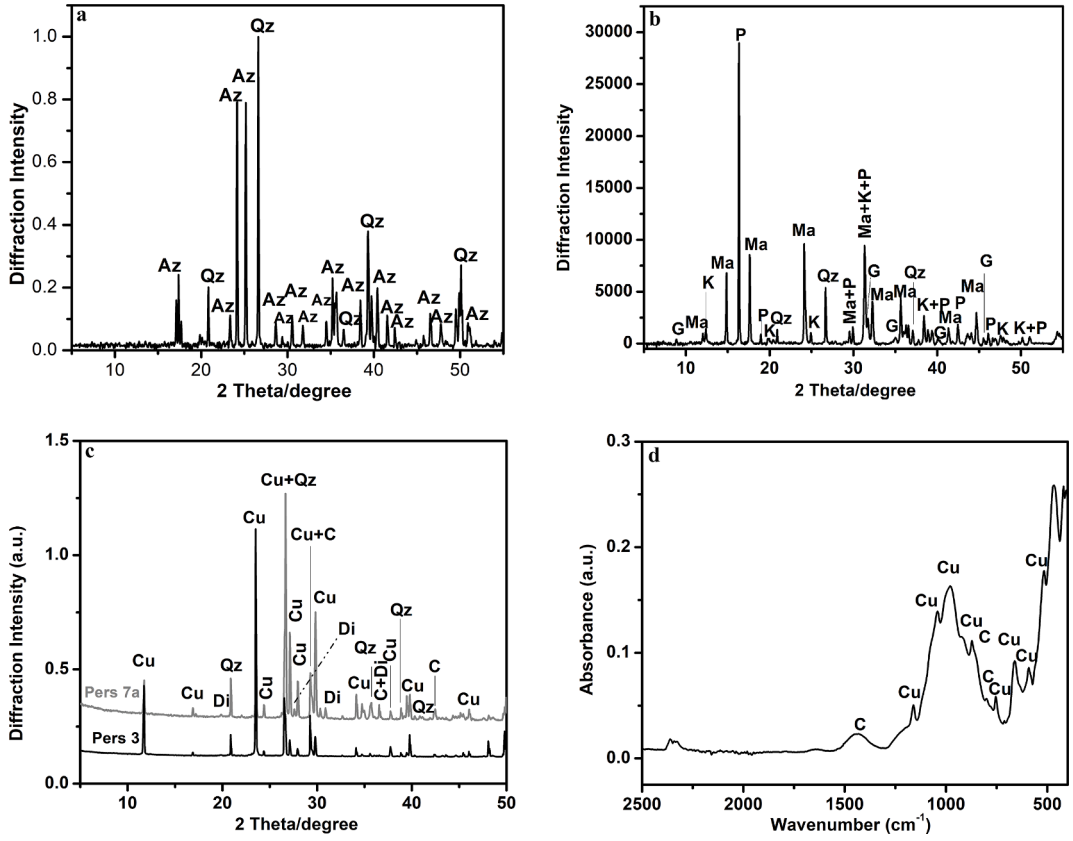

Fig. 2. (a) X-ray diffraction pattern (Az = azurite, Qz = quartz); (b) X-ray diffraction pattern (Ma = malachite, Qz = quartz, P = potassium magnesium silicate, G = glauconite, K = kaolinite); (c) X-ray diffraction pattern (Cu = cuprorivaite, Qz = quartz, Di = diopside, C = calcium carbonate); (d) ATR-FTIR spectrum.

with very high birefringence. They range in colour from blue to light blue or colourless. Rounded quartz particles (sample PERS3) and sometimes opaque minerals are visible. Calcite of secondary origin covers the external surface of the samples or fills some of the pores.

SEM morphological observations and EDS analysis (Table 2a, S3; Fig. S6b-c) also allowed to identify cuprorivaite (Egyptian blue) crystals

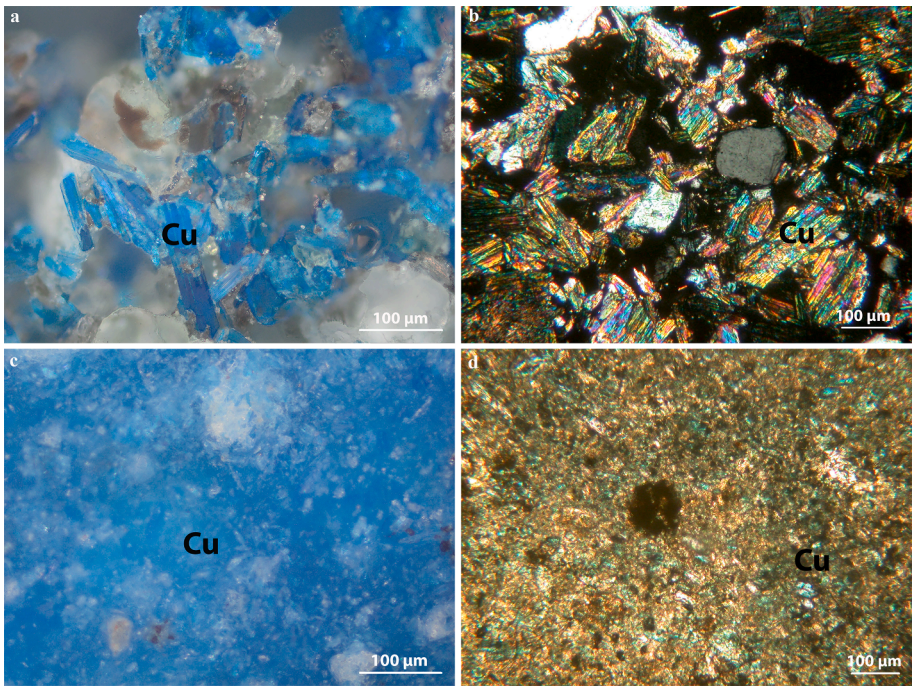

Fig. 3. Blue pellets: PLM micrographs in (a, c) reflected light; (b, d) transmitted light (XPL).

(light grey tone) and quartz particles (dark grey tone). Glassy phase (mid-grey hue) is present on the border of cuprorivaite crystals. The different crystals grain size of the samples is quite evident (Fig. S7a-c). The atomic percentage ratios of Si, Ca, and Cu achieved by EDS analysis (Table 3) are in agreement with the stoichiometry of cuprorivaite [37,38]. The CaO/CuO ratios range from 0.4 to 0.89 (Table 3). Low amount of K and Na were detected in a few samples. Na_2O/K_2O ratios range between 0.31 and 0.87%. Furthermore, Al, Mg Fe and Cr were identified as impurities. Hg and S particles, related to cinnabar/vermilion, were detected in sample PERS14. Cl was detected in PERS3, PERS3a and PERS15 probably related to Cu-chloride. Morphology and chemical composition of the thin crystals formed above the cuprorivaite crystals (samples PERS3a and PERS7a; Fig. S7d-e) attested the presence of Ca-Mg pyroxenes that was also confirmed by X-ray diffraction analysis (Table S2; Fig. S7f). Cuprorivaite ($CaCuSi_4O_{10}$) was detected as the main mineral phase (Table S2; Fig. 2c), together with quartz and calcite.

Egyptian blue presence was also confirmed both by ATR-FTIR analysis (Table 2a; Fig. 2d) because of its characteristic triplet at 1158, 1048 and 1008 cm^{-1}, attributed to antisymmetrical Si-O-Si stretching vibrations [39–41] and for the bands at 755 and 663 cm^{-1} due to the symmetrical Si-O-Si stretching [39]. It was also possible to identify in each blue sample the presence of calcium carbonate by its typical peaks at 1443, 876 and 715 cm^{-1} ascribable to ν_3, ν_2 and ν_4 respectively [42]. The presence of phyllosilicates with the asymmetric Si-O-Si stretching vibration around 980 cm^{-1} [43] was detected in sample PERS3a.

3.2. Yellow lumps

The yellow lumps (samples PERS1c, PERS2, PERS2a, PERS8, PERS9, PERS13; Table 1) vary in terms of colour and texture depending on their grain size and purity. Their shape ranges from slightly angular to round with a fine to coarse surface texture sometimes with two flattened sides (Fig. S3). ED-XRF analysis detected in all the samples Fe, Ca, Si, and K related to Fe-based pigments and Ca-based matrix (Table 2b).

According to DM and PLM observations, the particles grain size varies from fine (samples 1c; Fig. S8a) to very fine (samples 2, 2a, 8, 9; Fig. S8b–c). On the base of PLM and SEM/EDS investigations, a mixture of very fine-grained microcrystals of calcitized dolomite with

Table 3
Relative elemental compositions (average % weight ± standard deviation) of cuprorivaite crystals (EDS analyses normalised to 100%).

Sample code	Si	Ca	Cu	Ca/Cu
PERS3	48,42	20,38	31,2	0,65
	45,22	22,44	32,33	0,69
	54,4	20,06	25,54	0,78
	49,98	19,84	30,18	0,65
	52,78	13,44	33,78	0,4
	48,64	13,53	37,83	0,35
Average %	49,91	18,28	31,81	0,59
Standard deviation	3,29	3,83	4,07	0,17
PERS3a	46,44	21,32	32,24	0,66
	59,27	12,42	28,31	0,44
	41,28	19,11	39,6	0,48
Average %	49,00	17,62	33,38	0,53
Standard deviation	9,26	4,63	5,73	0,12
PERS7a	55,63	20,68	23,69	0,87
	55,84	20,62	23,54	0,87
Average %	55,74	20,65	23,62	0,87
Standard deviation	0,15	0,04	0,11	0
PERS14	53,46	19,17	27,37	0,7
	56,74	17,22	26,03	0,66
	47,96	15,1	36,94	0,41
	50,48	20,95	28,57	0,73
	52,22	17,62	30,17	0,58
	56,24	18,38	25,38	0,72
	36,16	28,08	35,76	0,78
Average %	50,47	19,50	30,03	0,65
Standard deviation	10,62	5,83	5,20	0,10
PERS15	51,88	19,78	28,34	0,69
	57,47	17,38	25,15	0,69
	52,93	21,36	25,71	0,83
	58,9	16,38	24,72	0,66
	54,02	19,67	26,32	0,74
	48,95	20,53	30,53	0,67
	46,12	22,81	31,07	0,73
	56,46	18,93	24,61	0,76
	58,86	16,81	24,33	0,69
	61,48	18,21	20,31	0,89
	55,25	18,8	25,96	0,72
	54,33	19,41	26,26	0,74
Average %	54,72	19,17	26,11	0,73
Standard deviation	3,89	0,60	3,35	0,09

rhombohedral and euhedral shape, calcite and rare quartz microcrystals were observed the sample PERS9 (Fig. 4a-b). Dolomite is partially altered in iron oxides, compatible with limonite. Sample PERS13 (Fig. S9a) consisting of carbonate matrix with micritic texture and rhombohedral phenocrysts having coarse grain size (ø 700–800 μ). The carbonate component is less evident on the edges and ooidal iron oxides prevail. The phenocrysts showing a very high birefringence are composed of magnetite and goethite. On the external surface, a carbonate- based patina and phyllosilicates are visible. EDS elemental distribution maps of sample PERS13 confirmed the presence of matrix composed of Ca, Si and Fe-based rhombohedral crystals, showing Si/Al-rich edges (Fig. S9b-c). According to EDS analysis (Tables 2b, S4), sample PERS1c is mainly composed of Fe and Si with a low amount of Al, K with Mg, Ti and Ca. Traces of P were found in samples PERS8, PERS2 and PERS13. Ba-based particles were identified in sample PERS2a. SEM-BSE micrograph and EDS map of sample PERS9 confirmed the presence of calcitized dolomite rhomboids with iron oxide rims and stains (Fig. S9d-e).

XRD analysis (Table 2b, S2) carried out in sample PERS1c identified the presence of quartz, goethite, kaolinite, calcite and muscovite (Fig. S10a) while only calcite and quartz were found in sample PERS2. Calcite, quartz, dolomite, muscovite and Fe-containing chlorite (chamosite /clinochlore) were detected in samples PERS8 and PERS9 (Fig. 5a, S10b). Albite and palygorskite were detected as minor phases respectively in sample PERS8 and sample PERS9.

The ATR-FTIR analysis showed in all these samples (Table 2b) the stretching vibrations of calcium carbonate [42] and silicates, such as kaolinite and quartz, as main components. In sample PERS1c (Fig. S10c) the signals at 914 cm^{-1} are due to goethite, the typical bands at 3692 and 3622 cm^{-1} of the OH stretching and the bands at 1109, 1001 and 789 cm^{-1} are related to kaolinite, while those at 534 and 455 cm^{-1} are ascribable to hematite [44]. The presence of both goethite (α-FeOOH) and hematite (α-Fe_2O_3) attested the mixture of red and yellow ochres [45,46]. Calcium carbonate and aragonite were identified in sample PERS8. The matrix is composed of quartz and calcium carbonate.

Raman analysis (Table 2b) allowed to identify yellow ochre in PERS1c (Fig. S10d) with characteristic features at 300, 390, 480 cm^{-1} belonging to goethite [47] and calcium carbonate in PERS1c PERS2, PERS2a and PERS9. Goethite and magnetite (Fe_3O_4) have been detected in PERS13.

3.3. Red lumps

The red lumps (samples PERS1a, PERS1b, PERS4b, PERS10, PERS11, PERS12; Table 1) are mostly rounded with a fine to coarse surface texture and sometimes with one flattened side (Fig. S3). They vary considerably in terms of colour, hue and shape depending on their grain size and purity (Fig. S11a-c).

ED-XRF analysis carried out on all the red lumps, detected mainly Fe, Si and Ca (Table 2c) indicating the presence of Fe-based pigments.

According to PLM and SEM/EDS investigations, the samples are generally composed by a variable mixture of iron oxides, red ochres, calcite crystals and carbonate matrix (Fig. S11d-e). In sample 4b, Fe-oxides showed features compatible with hematite (Fig. 4c-d), visible both in rhombohedral crystals with iron oxide rims with fine grain size (max 300 μ) or with very fine grain size mixed with calcite crystals (MGS = 30 μ) probably resulting from a dedolomitization process.

The high amount of Fe with low quantity of Si, Ca, K, Ti, Mg and Al detected by EDS analysis in the red samples (Table 2c, S5) confirm the presence of Fe-oxides red ochre and silicates. Cu-based particles were also found (Fig. S12a). Pb, Sb, (Fig. S12b), P and Ag were identified in sample PERS11 (Fig. S12c). Traces of As and P were detected in sample PERS1b.

The samples PERS1a and PERS12 (Fig. S13a) differs from others as they consist of marly limestone (part b) with red pigment (part a). The red pigment is composed of mono and polycrystals of quartz, mostly angular and varying in size, from a few microns to 600 μ mixed with opaque minerals, mainly hematite. The marly limestone is composed of a microcrystalline carbonate matrix, very fine minerals of clayey nature and opaque minerals. The crystals, estimated as a percentage of 5–10%, have a maximum size of 50 μ. SEM-EDS analyses and elemental maps of sample PERS12 (Fig. S13b) allowed to detect mainly Fe and Si in the red area (part a) and Ca, Si, Al in the white one (part b).

Quartz, calcite, dolomite, muscovite, palygorskite and Fe-containing

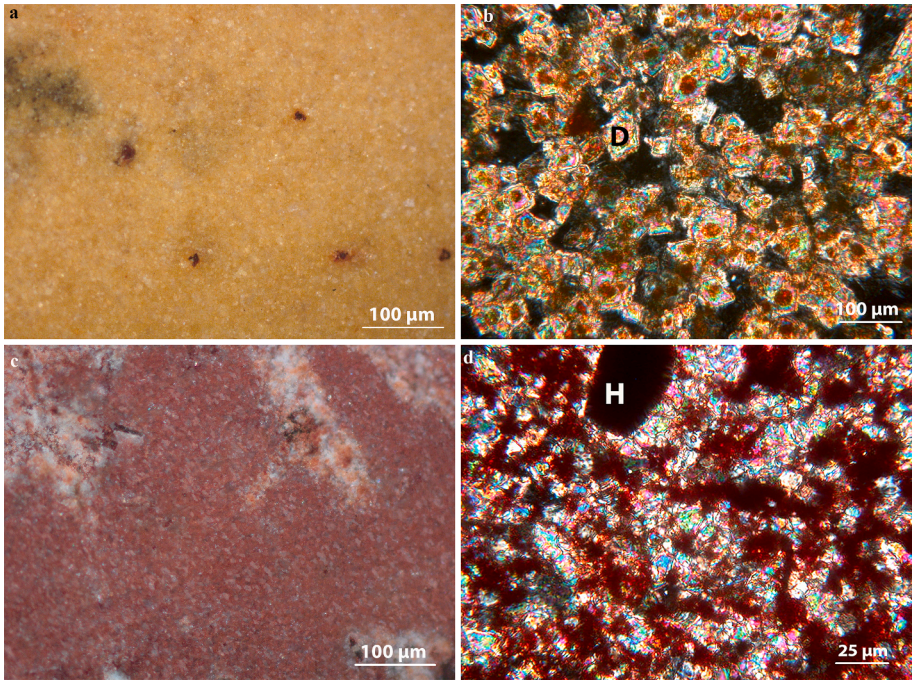

Fig. 4. Yellow lumps: PLM micrographs in (a) reflected light (XPL) and (b) transmitted light (XPL). Red lumps: PLM micrographs in (c) reflected light (XPL) and (d) transmitted light (XPL).

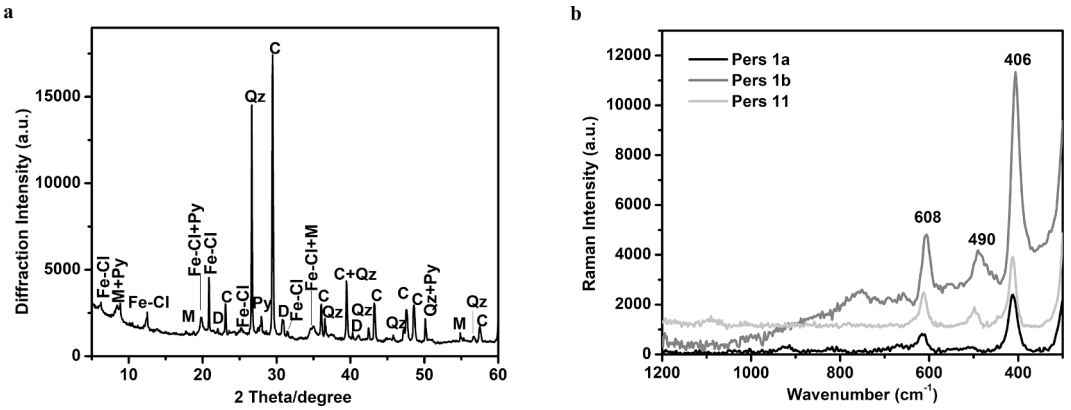

Fig. 5. (a) X-ray diffraction pattern (C = calcite, Qz = quartz, M = muscovite, D = dolomite, Fe-Cl = Fe-chlorite); (b) Raman spectra whit the typical bands of hematite (t = 700 ms, average = 15) (He = Hematite).

chlorite (chamosite /clinochlore) were detected by X-ray diffraction analysis in sample PERS12b (Table 2c, S2; Fig. S13c).

The presence of phyllosilicates was observed by ATR-FTIR analysis in several red samples (Table 2c), especially kaolinite (samples 1a, Fig. S14a). In PERS11, kaolinite, calcite, quartz, and aragonite with its characteristic bands at 1082 (ν_1) and 854 (ν_2) cm^{-1} [48] were detected by ATR-FTIR (Fig. S14b). The typical features of hematite (α-Fe_2O_3) at 530 and 450 cm^{-1} [44] were found in sample PERS1b together with the carbonyl stretching at 1740 cm^{-1} and methylenic signals at 2922 and 2850 cm^{-1} (Fig. S14c) which suggest the presence of lipid compound [49]. Goethite (α-FeOOH), calcium carbonate and kaolinite were identified in PERS10.

Raman analysis (Table 2c) evidenced in PERS4b the presence of red ochre and calcite, because of hematite weak signals at 300 e 410 cm^{-1}; in samples PERS1a, PERS1b and PERS11 the signals of hematite [50] were clearly detected (Fig. 5b).

3.4. Metal scrap

The colour of metal scrap (sample PERS6; Table 1) ranges from bright green to reddish (Figs. S3, S15a). ED-XRF analysis revealed a high amount of Cu-Sn in reddish areas and high Cu-Ca-Si amount in green ones (Table 2d).

According to PLM observation, a metallic matrix with scattered elongated and bright globular inclusions are visible in the central part of the thin section. Hexagonal grain structure randomly orientated is visible in the Cu-rich area after etching (Fig. S15b). Malachite microcrystals very fine-grained with poorly defined or pseudo-fibrous crystalline contours are present around the border. Cuprite was observed in the central red areas of the section. Hematite and probably magnetite are widespread in the sample. Rare Egyptian blue particles were observed (Fig. S15c). A carbonate-clay matrix with rare quartz crystals having a maximum size of 100–150 μ covered the external surface of the sample.

SEM-EDS data (Table 2d, S6) confirmed high Cu (71.58 to 93.14%) and low Sn (1.89 to 6.25%) content with lower percentages of Pb (0–3.39%) indicating a binary Cu-Sn bronze alloy (Fig. S16a-b). EDS analysis confirms the presence of cuprorivaite particles (Fig. S15d). Cu-based area with unreacted Si-particles and dendritic formations were observed (Figs. S16c-d).

4. Discussion

The use and the presence of brown, red, and yellow ochres are attested in Mesopotamia [23] whilst the sources of these coloured earth pigments were not undoubtedly identified. Other pigments as Egyptian blue, azurite, malachite, cinnabar, orpiment or realgar (arsenic-based) were supposed to be used only closely to their source areas. The localization of Egyptian blue manufacturing was considered by Moorey an open question linked to the development of ancient coloured frits in this area [23].

According to Nagel [15] a lot of archaeological evidence found in the archaeological sites of Mediterranean area and Near East, such as of pigments residues, palettes, pigment bowls, etc., should be to reconsider as they prove the presence of pigments production and painting activity. Moreover these evidences may be useful for understanding the manufacturing process and raw materials provenance.

Based on the results obtained by integrated analyses carried out on the colourful residues and bronze scrap unearthed in Persepolis West area we elaborated the aforementioned issue contributing with new results as follows.

4.1. Blue and green lumps

Azurite and malachite are hydrated copper carbonates generally formed in the upper oxidising zones of ore deposits at a low temperature and pH environments. They often represent a weathering product above copper-bearing sulphide deposits by the interaction of carbonated solutions with copper-rich minerals [51]. The copper-based carbonates were usually prepared by crushing, grinding, and washing them [52].

Concerning the azurite and malachite lumps found in Persepolis (samples PERS1 and PERS 4a), their composition suggested that quartz and Al-silicate occurs as natural impurity [53,54]. The green sample (PERS4a) is composed of malachite showing a typical prismatic-fibrous structure [52,53]. The presence of kaolinite and glauconite [55], belonging to those pigments labelled as green earth [56], could be evidence of a manufactured mixture (Table 3). The presence of clay minerals or other Fe-oxides, intentional or casual, changed in any case the colours of the original pigments. Cr traces are related to copper impurities attested in Iranian copper ores [57].

Regarding the presence of copper mines in Iran, it should be considered that the name azurite comes from an old Persian word, *lajvard*, meaning blue [58], in fact copper mines are widespread in this area [13,59,60]. Anarak is one of the oldest mines in Iran [61] from which have been extracted cuprite and malachite used as raw materials [62]. Malachite and azurite occur in the ancient Iran copper mine of Veshnaveh, between Qom and Kashan [63,64], as well as in the mines of Ahangaran (Ghaen), Chehel Kure (Baluchestan), Chah Moosa (Toroud), Abbasabad (Sabzevar) and Kerman area [59].

According to some scholars, the copper mines located in the Fars Province of Iran could be one of the possible geological sources of malachite used in the Persepolis area [24,65].

4.2. Egyptian blue pellets

Egyptian blue is the first man-made blue. It appeared at the beginning of 3000BC within Egyptian Kingdom and then it spread over the Mediterranean area from ca 2600BC [66,67].

To produce Egyptian blue, silica sand, lime and a small amount of alkali flux (natron or plant ash) were added to relatively pure copper ore, from metallic Cu or Cu-based alloy [68] and fired at about 850–1000 °C [69]. The sintering process allowed the formation of cuprorivaite crystals ($CaCuSi_4O_{10}$), partially-reacted quartz, and a glassy phase incorporating sometimes cuprite or tenorite [66,69].

In Persepolis West blue samples (PERS3, PERS3a, PERS7a, PERS14, PERS15), cuprorivaite was detected as the main mineral together with quartz and calcite as usually found in Egyptian blue [37,70]. CaO/CuO ratios of the investigated samples are typically in the range of Mesopotamian data [16,38,67,68,71,72], while the scarcity of K and Na could be ascribed to the loss of glass phase as a result of weathering. Furthermore, Fe, Al and Mg were detected as impurities suggesting the use of silicate-based sand as a possible source for quartz [68,73]. The different crystals size observed in the samples suggested diverse stages of Egyptian blue production. The deep blue coarse-grained crystals of cuprorivaite (as observed in samples PERS3) are the result of primary production from raw materials, whilst the light blue finer crystals (samples PERS14, PERS7 and PERS15) originated from various processing phases as grinding the frit, then remodelling to the required shape and re-firing, according to Panagiotaki et al. [74]. Egyptian blue pigment with light blue hue was also described by Theophrastus in the fourth century BC and reported by several authors [68,72,75,76].

This blue pigment has been widely used in ancient Iran [77]. Several Achaemenid objects excavated in the Persepolis Terrace are composed of Egyptian Blue [23]. Comparing the chemical composition of the investigated samples with these blue objects found in Persepolis the only difference is the tin absence [16,72].

As regards the provenance of the Egyptian blue pellets found in West Persepolis, the presence of pyroxenes, especially diopside, highly evidences the local manufacturing activity. These minerals form during the reaction of silica-rich glass and carbonates at a high temperature, thus during the production process [66,67]. Diopside does not usually appear within Egyptian blue artworks, whilst it is typically found as a kiln coating [42], within crucibles as firing material [78] or in their inner walls as a newly-formed phase due to the high firing temperature [79]. Diopside is often found in natural pigments as accessory mineral [80–82] but no evidence thereof emerged within Egyptian blue samples from decorations or painted surfaces. Furthermore, no evidence of diopside was recognized in the bulk of Egyptian blue when an excess of reagent was used [83]; its presence is rather improbable for at least two reasons:

- The temperature reported for the formation of Egyptian blue ranges from 870 °C to 1080 °C [74], being 870 °C the best conditions to achieve larger crystals [84]. Diopside forms at 950 °C [67] and it is more probable that within the crucible, higher temperatures are reached near the inner walls rather than in the bulk mixture, thus it is more reasonable that diopside forms in the very proximity of the crucible walls rather than in the bulk pigment.
- Diopside formation during the synthesis of Egyptian blue is usually ascribed to an excess of Ca. Still, if it occurs within the bulk mixture, it forms wollastonite, as for Egyptian green [66], whose traces were not recovered in our samples. Moreover, during the synthesis of Egyptian blue, the bulk of Ca and Cu are involved in forming cuprorivaite crystals any excess of Ca would be responsible for hindering cuprorivaite formation [66] which is instead the main component of our samples. An excess of Ca -which is anyway the source for diopside formation- is probably limited to some areas localized on crucible's walls experimenting higher temperatures respect to those of the bulk mixture.

Diopside presence in the Persepolis West samples should be therefore related to the Egyptian blue adhering to the crucible walls, indicating, thus, a local production of this material.

4.3. Yellow and red lumps

The use of ochres as pigments, mostly red, has been documented from Pleistocene to the present day. The term ochre refers to rocks whose composition is generally represented by two forms of iron oxide (Fe_2O_3 and FeO) mixed with clays, silicates and other minerals ranging in colour from deep purple to light yellow, being blood red the most common hue used in ancient times [85,86]. It is known that the red hue is caused by the fine-grained hematite and the yellowish coloration may be due to fine-grained hydroxide, moreover the colour varies depending on the particles size and their uniformity [54].

Based on the investigation of the Persepolis West lumps, goethite and magnetite were found in yellow samples (PERS1c, PERS2, PERS2a, PERS8, PERS9, PERS13), while hematite occurs in various amounts in the red ones (PERS1a, PERS1b, PERS4b, PERS10, PERS11, PERS12). The presence of quartz, calcite, Fe-chlorite, dolomite, aragonite, albite, and phyllosilicates, such as kaolinite, muscovite, and palygorskite were also detected.

The occurrence of iron oxides/hydroxides in crystalline (hematite, goethite and magnetite) or amorphous form (limonite), as well as calcite, quartz and aluminosilicates (feldspar and various clay minerals) in ochre pigments, is quite common [87]. Their presence points out the local origin of earth pigments because they are the more abundant minerals found in the geological environment.

The provenance of archaeological ochres is a matter of debate as it has been generally considered the geographical proximity rather than the specific mineralogical and microscopic features of Fe-based pigments [88]. Several scholars used to distinguish the different ochre source using elemental fingerprints, such as trace and rare earth elements, [85,89] to satisfy the provenance postulate [90].

In order to collect information on the possible sources, the presence of distinctive features in the yellow and red lumps found in Persepolis West was therefore considered.

Firstly, the presence of rhombohedral Fe-based crystals observed in the lumps of pigments (samples PERS4b and PERS13) is also attested in the Dehbid iron deposit, located northeast of Shiraz, in south Iran. According to Rajabzadeh & Rasti [91], the Dehbid deposits are inside the metasedimentary rocks of the late Paleozoic era and silicified dolomite of the early Mesozoic era. In the ores there are a large amount of magnetite, whilst hematite, goethite, specularite and martite are secondary. Dolomite, microcrystalline quartz, amphibole and minor chlorite are associated with Fe mineralization in brecciated zones suggesting a hydrothermal origin for ores [91].

Furthermore, in our research the ooidal iron oxides were taken into consideration, together with the presence of Fe-containing chlorite. The ooidal shapes are typical of several iron ores [92] and the Fe-containing chlorite was found in most of the Palaeozoic ironstones [93]. Clinochlore, belonging to the chlorite group, has also been detected in red pigments found in the settlements of Akrotiri, Thera [87]. Chamosite, a Fe-containing chlorite, was detected in sedimentary formation of Iranian ooidal ironstone [94].

Additionally, we should mention the presence of calcitized dolomite rhombs with iron-oxide stains surrounding the calcite grains (sample PERS9) as described by Sajó et al. [88]. According to Vandeginste & John [95], the dedolomitization process (i.e. calcitization of dolomites) can occur in different degrees and modes causing two different textures: a) oxidation of dolomite and dolomite recrystallization, resulting in a goethite-recrystallized dolomite fabric; b) oxidation and calcitization of dolomite causing a goethite–dedolomite fabric as in the case of the Persepolis West samples. In Iranian dolomite rocks, the presence of both the calcitization process and the ferruginous dolomite has been confirmed [96] but further investigation will be required to confirm the provenance.

It should lastly be pointed out that Pb, Sb and Cu identified in Fe-

based red lumps can be related to craftsmen manufacturing activity on metals [42,97] or they could even indicate a hydrothermal origin [98]. The Ag particles could suggest a connection with lead or silver mines as Vitruvius and Pliny mentioned the presence of ochre (*sil*) in silver quarries [42]. It could also be linked to the phenomenon of adsorption on iron oxides and hydroxides [46,99].

The presence of phyllosilicates, such as muscovite, kaolinite and palygorskite in the Persepolis West samples (red and yellow lumps) bring us back to the controversial question reported by Hradil et al. [56] related to a different or common origin of clay minerals and iron oxides in ochres. It should be noted that muscovite has been identified in the yellowish paint on plaster fragments found in Achaemenid Pasargadae and Persepolis [24]. Kaolinite and goethite have been found in several archaeological sites mixed with red ochre and red hematite [100,101]. Judson suggested the use of kaolinite added to hematite as an extender pigment in late Palaeolithic excavations [102]. It must be emphasised, however, that kaolinite is already attested in the bauxitic-lateritic deposits southeast of the Kerman city, in Iran [94]. Palygorskite, a magnesium aluminium phyllosilicate, has been detected in high amounts in arid and semi-arid regions of Fars Province [103].

Regarding the aragonite detected in yellow and red samples, its origin is not clear as it is present in Cretaceous Iranian carbonates in Fars area [104] or it could be related to the iron ore deposits [51,69].

The appearance and shape of the Persepolis West lumps vary in terms of colour, size and grains. The colours range from light yellow to dark red. They show one or two flattened sides and rounded profiles suggesting that they could have been submitted to a previous purification step(s) during production.

Froment et al. [105] described that after the selection of the ores the pigments were extracted and prepared as usual. Indeed, the treatment used to enrich the pigments and to remove the impurities involved raw materials washing and subsequent drying [54]. To use the pigments, they have to be ground to powder and to transport them they have to be assembled in lump, pellet and cake forms that are easier for trading purposes [106]. The rounded shape and one or more flat surface of the lumps suggest a shaping process while moist or turning it over, during the manufacturing process [42,107].

The presence of lipid compound detected in a red lump could be related to the use of proteinaceous substances in order to obtain a sticky product [108]. In brown ochre of Tell-Amarna (Egypt), the presence of terpene-type resin binder was justified with the necessity to increase adhesion properties for a specific application or to darken the pigments hue [50].

4.4. Metal scrap

In the tin bronze scrap unearthed in Persepolis West (sample PERS6) a few amounts of lead (0–3.39%) was detected. Copper hexagonal grain structure observed in the sample can be related to extremely slow cooling [33] whilst the dendritic morphology is due to the rapid growth of the crystal following energetically favourable directions. According to Tiller [109] a slight change in environmental conditions can generate different morphology during the crystals growth.

The presence of lead could indicate impurities related to the use of Cu-based minerals instead of native copper. Lead and zinc, such as alkaline substances, silicates and iron oxides, were sometimes added as fluxes to lower the melting point during the working process.

Lead was found in several Iranian bronze objects dating between c.1500-550BC [63,110,111]. In the manufacturing of the Achaemenid metal trumpet, preserved in the Persepolis Museum [112] a tin-bronze alloy with small amounts of zinc was used [113]. The metallurgical remains found in Persepolis West are composed of tin bronzes with variable amounts of lead [114].

The presence of Egyptian blue crystals identified in the bronze scrap (sample PERS6) could indicate a local manufacturing activity to produce the synthetic blue pigment according to the use of bronze waste or corrosion products as a source of copper [69,72].

The provenance of bronze is an open question which has not yet been fully revealed even if several studies have been carried out. Previous studies attested that it was not clear if Iranian bronze was imported as ingots from elsewhere or it was manufactured using raw materials from the local copper mines [23]. Anatolia, Cyprus, Iran, and the Persian Gulf are considered the major copper source areas in the Near East. The copper used in Sumer and Babylonia is attested to come from ancient Iran and the Persian Gulf [23]. In his review, Oudbashi et al. [110] clarified the role of archaeometallurgy in Iran providing a lot of information on the development of metallurgy including ancient ore mining, metallurgical remains, artefacts, technologies and compositions. Ancient bronze production of various artefacts is attested in the Iranian Plateau especially in Luristan in west of Iran [115,116]. Several investigations were carried out on various Iranian bronze objects suggesting the production of binary Cu-Sn alloy, especially in the Iron Age [111,116]. The hypothesis [114] related to the use of Jian copper mine, in the Sanandaj–Sirjan area about 120 km from Persepolis, as the copper source for producing the Persepolis bronze objects still has to be proved.

5. Conclusions

Based on the discovery of the coloured residues in the recent Iranian-Italian excavations at Persepolis West, the multidisciplinary investigations verified and confirmed the archaeologists' hypothesis related to a local manufacturing activity dedicated to pigments production in the craft zone discovered at Persepolis West, an area close to the Persepolis Terrace.

Lumps of azurite, malachite (with glauconite), red and yellow ochres (hematite, magnetite, goethite, limonite) together with pellets of Egyptian blue are most likely related to the painting palette identified in the Persepolis Terrace and to the decorating activity of the nearby Imperial and élite buildings.

The mineralogical composition and microscopic features of the lump of pigments, such as azurite, malachite, red and yellow ochres have common characteristics with local raw materials indicating a possible use of close sources. Many of the lumps show a typical rounded shape with one or more flattened side, both indicative of a shaping process.

The presence of pyroxenes (byproducts) in the Egyptian blue pellets and the occurrence of Egyptian blue crystals within the bronze scrap constitute further indication for a local manufacture of the synthetic blue pigment. Craftsmen activity of metal processing was also testified by the presence of Ag, Cu and As within Fe-based red lumps.

This paper demonstrates how a careful analysis of unearthed coloured materials (lumps and pellets of pigments, and scrap metal) can often tell more about production techniques, pigments provenance and making of parietal artworks than the artworks themselves. Specific mineralogical and microscopic features are often crucial in establishing both sources and manufacturing processes, disclosing whether a pigment is imported or locally produced. In this way we could find out more about both the artistic trades and trends in ancient history. Thus, new routes are drawn by following the transformation processes of materials which frequently spread over many countries, leaving their traces as a perpetual witness.

CRediT authorship contribution statement

Maria Letizia Amadori: Conceptualization, Methodology, Investigation, Data curation, Writing - original draft, Writing - review & editing, Supervision, Funding acquisition. **Manuela Vagnini:** Investigation, Writing - review & editing. **Riccardo Vivani:** Investigation. **Chiara Anselmi:** Data curation, Writing - original draft, Writing - review & editing. **Alireza Askari Chaverdi:** Resources. **Pierfrancesco Callieri:** Resources. **Emad Matin:** Resources, Writing - review & editing. **Valeria Mengacci:** Investigation, Data curation, Writing - original draft, Writing - review & editing.

Declaration of Competing Interest

The authors declare that they have no known competing financial interests or personal relationships that could have appeared to influence the work reported in this paper.

Acknowledgements

This research was carried out in the framework of the project 'From Palace to Town', thanks to the Iranian-Italian Joint Archaeological Mission in Fars of the Department of Cultural Heritage of the University of Bologna, the ISMEO, the Iranian Centre for Archaeological Research, the Persepolis World Heritage Foundation and the Shiraz University. Thanks are due to Valentina Raspugli for providing samples preparation. Thank you to anonymous reviewers for thoughtful and thorough commentary.

Appendix A. Supplementary data

Supplementary data to this article can be found online at https://doi.org/10.1016/j.microc.2021.106304.

References

[1] A. Sh. Shahbazi, Persepolis. Encyclopaedia Iranica online, PERSEPOLIS – Encyclopaedia Iranica (iranicaonline.org), 2012 (Accessed: 29 September, 2019).
[2] R. Boucharlat, T. D. Schacht, S. Gondet, Surface Reconnaissance in the Persepolis Plain (2005-2008). New Data on the City Organization and Landscape Management, in: G.P. Basello, A.V. Rossi (Eds.), Dariosh Studies II. Persepolis and Its Settlements: Territorial System and Ideology in the Achaemenid State. Dipartimento Asia, Africa e Mediterraneo, Series minor, LXXVIII, Università 'L'Orientale', Napoli, 2012, pp. 249, 256-260, 290.
[3] S. Gondet, K. Mohammadkhani, A. Askari Chaverdi, A newly discovered building complex north of the "Frataraka" Complex. Consequences for the spatial definition of the Persepolis-Parsa Royal Area. Arta 2018.003, 1–35, http://www.achemenet.com/pdf/arta/ARTA_2018.003-Gondet-Mohammadkhani-Askari.pdf (Accessed: 2 May, 2020).
[4] B. Aminpour, S. Gondet, K. Mohammadkhani, Geophysical surveys over Persepolis Northwest area: an overview, in: A. Askari Chaverdi, P. Callieri, Persepolis West (Fars, Iran). Report on the Fieldwork carried out by the Iranian-Italian joint Archaeological mission in 2008–2009, BAR-IS-2870, BAR Publishing, Oxford, 2017, pp. 4–25.
[5] A. Askari Chaverdi, P. Callieri, The activities of the Iranian–Italian Joint Archaeological Mission at Persepolis West (Fars, Iran): first result of the studies on the pottery of Achaemenid and post Achaemenid age, in: G. P. Basello, A.V. Rossi (Eds.), Dariosh studies II: Persepolis and its settlements: territorial system and ideology in the Achaemenid state. Dipartimento Asia, Africa e Mediterrano, Series minor, LXXVIII, Università 'L'Orientale', Napoli, 2012, pp. 230–239.
[6] A. Askari Chaverdi, P. Callieri, Persepolis West (Fars, Iran): Report on the fieldwork carried out by the Iranian-Italian joint archaeological mission in 2008-2009, BAR-IS-2870, BAR Publishing, Oxford, 2017, pp. 286–288.
[7] A. Mercuriali, Area B, Trench Tr. 4, in: A. Askari Chaverdi, A., Callieri, P., Persepolis West (Fars, Iran). Report on the Fieldwork carried out by the Iranian-Italian joint Archaeological mission in 2008–2009, BAR-IS-2870, BAR Publishing, Oxford, 2017, pp. 48–67, 51, 59.
[8] C. Nylander, Achaemenid imperial art, in: M. Trolle Larsen (Ed.), Power and propaganda. A Symposium on Ancient Empires, Akademisk Forlag, Copenhagen, 1979, pp. 345–359.
[9] W.F.M. Henkelman, Anhang: Egyptians in the Persepolis Archives, in: M. Wasmuth (Ed.), Ägypto-persische Herrscher-und Herrschaftspräsentation in der Achämenidenzeit, Oriens et Occidens (27), Stuttgart, 2017, pp. 278–280.
[10] E.F. Schmidt, Persepolis, 1 Structures, reliefs, inscriptions, The University of Chicago Oriental Institute publications, University of Chicago Press, Chicago, Ill, 1953, pp. 71, 77-78, 122, 191–263.
[11] F.R. Matson, A study of wall plaster, flooring, and bitumen, in: Schmidt, E.F., Persepolis, vol. I: Structures, Reliefs, Inscriptions, University of Chicago Press, Chicago, fn. 4, 1953, p. 133.
[12] A.B. Tilia, Studies and restorations at Persepolis and other sites of Fārs II. ISMEO Reports and Memoirs 18, Rome, 1978, pp. 29–70, 68–79.
[13] L. Stodulski, E. Farrel, R. Newman, Identification of ancient Persian pigments from Persepolis and Pasargadae, Stud. Conserv. 29 (3) (1984) 143–149, https://doi.org/10.2307/1506017.
[14] A. Nagel, Color and gilding in Achaemenid Architecture and sculpture, in: D.T. Potts (Ed.), The Oxford Handbook of Ancient Iran, Oxford University Press, Oxford, 2013, pp. 596–611.
[15] A. Nagel, Painters' workshop in the Ancient Near East: a reassessment, in: S. Gondet, E. Haerink (Eds.), L'Orient est son jardin: hommage à Remy Boucharlat, Acta Iranica 58, Peeters Publishers, Leuven, 2018, pp. 382–383.
[16] F.R. Matson, Egyptian Blue, in: E.F. Schmidt, Persepolis, vol. II: Contents of the Treasury and other discoveries. OIP 69, Chicago, 1957, pp.133–135.
[17] A. Askari Chaverdi, T.D. Potts, Archaeological Excavation from Qal-e Qali, Unpublished Report, Iranian Center for Archaeological Research, ICAR, (Archive), 2010.
[18] A. Nagel, Colors, gilding and painted motifs in Persepolis: approaching the polychromy of Acheamenid Persian Architectural Sculpture, C. 520-330 BCE, Degree Dissertation, University of Michingan, 2010, pp.108-109, 252–256.
[19] R. Boucharlat, Susa iii. The Achaemenid period. Encyclopedia Iranica online, http://www.iranicaonline.org/articles/susa-iii-the-achaemenid-period, 2009 (Accessed: 29 September, 2019).
[20] L. Colliva, E. Matin, Other finds: inventoried objects, in: A. Askari Chaverdi, P. Callieri, Persepolis West (Fars, Iran). Report on the Fieldwork carried out by the Iranian-Italian joint Archaeological mission in 2008–2009, BAR-IS-2870, BAR Publishing Oxford, 2017, pp. 236, 253–254.
[21] G. Verri, P. Collins, J. Ambers, T. Sweek, St.J. Simpson, Assyrian colours: pigments on a neo-Assyrian relief of a parade horse, The British Museum Technical Bulletin 3 (2009) 57–62.
[22] S. Thavapalan, A World in color, polychromy of Assyrian sculpture, in: A. W. Lassen, E. Frahm, K. Wagensonner (Eds.), Ancient Mesopotamia Speaks: highlights of the Yale Babylonian Collection, Yale University Press, 2019.
[23] P.R.S. Moorey, Ancient Mesopotamian materials and industries, Oxford University Press, Oxford, 1994, pp. 186–189, 327.
[24] J.C. Ambers, St. J. Simpson, Some pigment identifications for objects from Persepolis. Arta 02:1-13, http://www.achemenet.com/pdf/arta/2005.002-Ambers-Simpson.pdf , 2005 (Accessed: 17 November, 2019).
[25] D. Stronach, Pasargadae: A report on the excavations conducted by the British Institute of Persian Studies from 1961 to 1963, Clarendon Press, Oxford, 1978, p. 85.
[26] E. Aloiz, J.G. Douglas, A. Nagel, Painted plaster and glazed brick fragments from Achaemenid Pasargadae and Persepolis, Iran, Herit. Sci. 4 (2016) 2–6, https://doi.org/10.1186/s40494-016-0072-7.
[27] A. Tadjvidi, Dānestaniha-ye novin darbāre-ye honar va bāstānšenāsi-e asr haxāmaneši, bar bonyād kāvoshā-ye panj sāleh Taxt-e Jamšid [New Data on Achaemenid Art and Archaeology after Five Years of Excavations at Persepolis]. Tehran: Az entešārāt-e edāre-ye kol negāreš-e vezārat-e farhang va honar-e Iran (in Persian), 1968–1972, Tehran: Iranian Ministry of Culture and Arts (in Persian), 1976, pp. 97-102.
[28] H. Rahsaz, A Lapis Lazuli like Object found during the excavation of the canals of the Persepolis Terrace in 1381 (2002-2003). Translated from Persian and annotated by E. Matin, in: S. Badalkhan, G.P. Basello, M. De Chiara (Eds), Iranian studies in Honour of Adriano V. Rossi, Part two. Series Minor, 87/2, Napoli, 2019, pp. 753–755.
[29] S. Razmjou, Glazed Bricks in the Achaemenid Period" (in German and English), in: T. Stoellner, R. Slotta & R. Vatandoust (Eds.), Persien Antike Pracht, Deutsches Bergbau-Museum, Bochum (2004) 382–393.
[30] A. Askari Chaverdi, P. Callieri, E. Matin, Tol-e Ajori, A Monumental Gate of the Early Achaemenian period in the Persepolis Area. The excavation season of the Iranian- Italian project "From Palace to Town", Archäol. Mitteilungen aus Iran und Turan 46 (2014) (2014) 223–254.
[31] A. Askari Chaverdi, P. Callieri, E. Matin, The Monumental Gate at Tol-e Ajori, Persepolis (Fars): New Archaeological Data, Iran. Antiq. 52 (2017) 205–258.
[32] M.L. Amadori, P. Pallante, P. Fermo, M.A. Emami, A.A. Chaverdi, P. Callieri, E. Matin, Advances in Achaemenid brick manufacturing technology: evidence from the Monumental Gate at Tol-e Ajori (Fars, Iran), Appl. Clay. Sci. 152 (2018) 131–142, https://doi.org/10.1016/j.clay.2017.11.004.
[33] D.A. Scott, Metallography and Microstructure of Ancient and Historic Metals, The J.P. Getty Trust, Singapore, 1991, pp. 5–8.
[34] J.B. Cooper, M. Abdelkader, K.L. Wise, Sequentially shifted excitation Raman spectroscopy: novel algorithm and instrumentation for fluorescence-free Raman spectroscopy in spectral space, Appl. Spectrosc. 67 (8) (2013) 973–998, https://doi.org/10.1366/12-06852.
[35] J.B. Cooper, S. Marshall, R. Jones, M. Abdelkader, K.L. Wise, Spatially compressed dual-wavelength excitation Raman spectrometer, Appl. Opt. 53 (11) (2014) 3333–3340, https://doi.org/10.1364/AO.53.003333.
[36] A. Kostomitsopoulou Marketou, F. Andriulo, C. Steindal,S: Handberg, Egyptian Blue Pellets from the First Century BCE Workshop of Kos (Greece): Microanalytical Investigation by Optical Microscopy, Scanning Electron Microscopy-X-ray EnergyDispersive Spectroscopy and Micro-Raman Spectroscopy, Minerals 10 (2020) 1063. 10.3390/min10121063.
[37] M.H. Mahmoud, A preliminary investigation of ancient pigments from the mortuary temple of Seti I, El-qurna (Luxur, Egypt), MAA 11 (1) (2011) 99–106.
[38] H.G. Wiedemann, G. Bayer, A. Reller, Egyptian blue and Chinese blue: production technologies and applications of two historically important blue pigments, in: S. Colinart, M. Menu (Eds.), La couleur dans la peinture et l'émaillage de l'Égypte ancienne, Edipulgia, Bari, 1998, pp. 195–203.
[39] H. El-Gaoudy, N. Kourkoumelis, E. Varella, D. Kovala-Demertzi, The effect of thermal aging and color pigments on the Egyptian linen properties evaluated by physicochemical methods, Appl. Phys. A 105 (2011) 497–507, https://doi.org/10.1007/s00339-011-6507-9.
[40] M.H. Mahmoud, L. Papadopoulou, Archaeometric analysis of pigments from the Tomb of Nakht-Djehuty (TT189), El-Qurna Necropolis, Upper Egypt, ArcheoSciences 37 (2013) 19–33, https://doi.org/10.4000/archeosciences.3967.
[41] M.H. Mahmoud, Investigations by Raman microscopy, ESEM and FTIR-ATR of wall paintings from Qasr el-Ghuieta temple, Kharga Oasis, Egypt, Herit. Sci. 2 (2014) 18–29, https://doi.org/10.1186/s40494-014-0018-x.

[42] A. Kostomitsopoulou Marketou, K. Kouzeli, Y. Facorellis, Colourful earth: iron-containing pigments from the Hellenistic pigment production site of the ancient agora of Kos (Greece), J. Archaeol. Sci. Rep. 26 (2019) 101843–101856, https://doi.org/10.1016/j.jasrep.2019.05.008.

[43] T. Toupance, M. Kermarec, J-F. Lambert, C. Louis, Conditions of formation of copper phyllosilicates in silica-supported copper catalysts prepared by selective adsorption, J. Phys. Chem. B (2002), 106, 9, 2277–2286. doi.org/10.1021/jp013153x.

[44] R. Linn, Layered pigments and painting technology of the Roman wall paintings of Caesarea Maritima, J. Archaeol. Sci. Rep. 11 (2017) 774–781, https://doi.org/10.1016/j.jasrep.2016.12.018.

[45] C. Genestar, C. Pons, Earth pigments in painting: characterisation and differentiation by means of FTIR spectroscopy and SEM-EDS microanalysis, Anal. Bioanal. Chem. 382 (2005) 269–274, https://doi.org/10.1007/s00216-005-3085-8.

[46] R.M. Cornell, U. Schwertmann, The Iron Oxides: Structure, Properties, Reactions, Occurrences and Uses, Wiley-VCH Verlag GmbH & Co. KGaA, Weinheim, 2003, 10.1002/jrs.1187.

[47] J. Ambers, Raman analysis of pigments from the Egyptian Old Kingdom, J. Raman Spectrosc. 35 (2004) 768–773, https://doi.org/10.1002/jrs.1187.

[48] D. Chakrabarty, S. Mahapatra, Aragonite crystals with unconventional morphologies, J. Mater. Chem. 9 (1999) 2953–2957, https://doi.org/10.1039/A905407C.

[49] G. Socrates, Infrared and Raman Characteristic Group Frequencies: Tables and Charts, third ed., Wiley, New York, 2004.

[50] A.R. David, H.G.M. Edwards, D.W. Farwell, D.L.A. De Faria, Raman spectroscopic analysis of ancient egyptian pigments, Archaeometry 43 (2001) 461–473, https://doi.org/10.1111/1475-4754.00029.

[51] N. Eastaugh, V. Walsh, T. Chaplin, R. Siddall, Pigment Compendium: a dictionary and Optical Microscopy of historic pigments, 1st ed. Butterworth-Heinemann, London, 2008, pp. 39-80, 152, 285.

[52] R.J. Gettens, E. West Fitzhugh, Malachite and green verditer, Stud. Conserv. 19 (1974) 2–23.

[53] G. Balassone, C. Petti, N. Mondillo, T.L. Panikorovskii, R. De Gennaro, P. Cappelletti, A. Altomare, N. Corriero, M. Cangiano, L. D'Orazio, Copper minerals at Vesuvius Volcano (Southern Italy): a mineralogical review, Minerals 9 (2019) 730, https://doi.org/10.3390/min9120730.

[54] R. Siddal, Mineral pigments in Archaeology: their analysis and the range of available materials, Minerals 8 (2018) 201–236, https://doi.org/10.3390/min8050201.

[55] V.A. Drits, L.G. Dainyak, F. Muller, G. Besson, A. Manceau, Isomorphous cation distribution in celadonites, glauconites and Fe-illites determined by infrared, Mössbauer and EXAFS spectroscopies, Clay Miner. 32 (1997) 153–179, https://doi.org/10.1180/claymin.1997.032.2.01.

[56] D. Hradil, T. Grygar, J. Hradilová, P. Bezdička, Clay and iron oxide pigments in the history of painting, Appl. Clay Sci. 22 (2003) 223–236, https://doi.org/10.1016/S0169-1317(03)00076-0.

[57] S. Jannesar Malakooti, S.Z. Shafaei Tonkaboni, M. Noaparast, Characterisation of the Sarcheshmeh copper mine tailings, Kerman province, Southeast of Iran, Environ. Earth Sci. 71 (2014) 2267–2291, https://doi.org/10.1007/s12665-013-2630-6.

[58] G. Rapp, Archaeomineralogy, Springer-Verlag, Berlin Heidelberg, 2009, pp. 164–165.

[59] W.R. Gocht, H. Zantop, R.G. Eggert, Mineral deposits and metallogenic concepts, in: International Mineral Economics, Springer-Verlag, Berlin, Heidelberg, 1988, p. 147, https://doi.org/10.1007/978-3-642-73321-5_2.

[60] N. Nezafati, E. Pernicka, M. Momenzadeh, Iranian ore Deposit and Their Role in the Development of Ancient Cultures, Der Anschnitt, Anatolian Metal IV (Beiheft 21), Dt. Bergbau Museum, Bochum, 2008, pp. 77–90.

[61] T.A. Wertime, The beginnings of metallurgy: A new look: Arguments over diffusion and independent invention ignore the complex metallurgic crafts leading to iron, Science 182 (4115) (1973) 875–887, https://doi.org/10.1126/science.182.4115.875.

[62] M. Ghorbani, The Economic Geology of Iran, Mineral Deposits and Natural Resources, Springer, 2013, pp. 53-61, 78, 103-195.

[63] P.R.S. Moorey, Archaeology and pre-Achaemenid metalworking in Iran: a fifteen-year retrospective, Iran, BIPS 20 (1) (1982) 81–101.

[64] M. Momenzadeh, H.W. Walther, Mineral deposits and metallogenic epochs in the area of the Geotraverse across Iran – a review, Neues Jahrbuch für Geologie und Paläontologie – Abhandlungen Band 168 Heft 2-3 (1984) 468-478. 10.1127/njgpa/168/1984/468.

[65] M. Emami, "Toroud", The late motion for As-Sb bearing Cu production from 2nd millennium BC in Iran: An archaeometallurgical approach, MAA 14 (2) (2014) 169–188.

[66] C. Grifa, L. Cavassa, A. De Bonis, C. Germinario, V. Guarino, F. Izzo, I. Kakoulli, A. Langella, M. Mercurio, V. Morra, Beyond Vitruvius: new insight in the technology of Egyptian blue and green frits, J. Am. Ceram. Soc. 99 (2016) 3467–3475, https://doi.org/10.1111/jace.14370.

[67] O. Oudbashi, M. Hessari, A "Western" imported technology: an analytical study of the Achaemenid Egyptian blue objects, J. Cult. Herit. 47 (2021) 246–256. https://www.sciencedirect.com/science/article/pii/S1296207420304854.

[68] G.D. Hatton, A.J. Shortland, M.S. Tite, The production technology of Egyptian blue and green frits from second millennium BC Egypt and Mesopotamia, J. Archaeol. Sci. 35 (6) (2008) 1591–1604, https://doi.org/10.1016/j.jas.2007.11.008.

[69] D.A. Scott, A review of ancient Egyptian pigments and cosmetics, Stud. Conserv. 61 (4) (2016) 185–202, https://doi.org/10.1179/2047058414Y.0000000162.

[70] I. Kakoulli, Egyptian blue in Greek painting between 2500 and 50 BC, in: A. J. Shortland, I.C. Freestone, T. Rehren (Eds.), From Mine to Microscope, Oxbow Books, Oxford, UK, Advances in the Study of Ancient Technology, 2009, pp. 79–84.

[71] A.J. Shortland, K. Eremin, The analysis of second millennium glass from Egypt and Mesopotamia, Part 1: new WDS analyses, Archaeometry 48 (4) (2006) 581–603, https://doi.org/10.1111/j.1475-4754.2006.00274.x.

[72] J. Riederer, Egyptian blue, in: E. West Fitzhugh (Ed.), Artist's pigments - A handbook of their history and characteristics, vol. 3, National Gallery of Art Washington, Archetype Publications, London, 1997, pp. 23–40.

[73] S. Pagès-Camagna S. Colinart, The Egyptian Green pigment: its manufacturing process and links to Egyptian Blue, Archaeometry, 45 (4) (2003) 637-58. 10.1046/j.1475-4754.2003.00134.x.

[74] M. Panagiotaki, M. Tite, Y. Maniatis, Egyptian Blue in Egypt and Beyond: The Aegean and the Near East, in: P. Kousoulis, N. Lazaridis (Eds.), Proceedings of the Tenth International Congress of Egyptologists, University of the Aegean, Rhodes 22-29 May 2008 II, Peeters Publishers, Louvain, 2015, pp.1769–1789.

[75] S. Pagès-Camagna, S. Collinart, C. Coupry, Fabrication processes of archaeological Egyptian blue and green pigments enlightened by Raman microscopy and scanning electronic microscopy, J. Raman Spectrosc. 30 (1999) 313–317, https://doi.org/10.1002/(SICI)1097-4555(199904)30:4<313::AID-JRS381>3.0.CO;2-B.

[76] T. Katsaros, I. Liritzis, N. Laskaris, Identification of Theophrastus' pigments *egyptios yanos* and *psimythion* from archaeological excavations, ArcheoSciences 34 (2010) 69–80, https://doi.org/10.4000/archeosciences.2632.

[77] H. Berke, Chemistry in ancient times: the development of blue and purple pigments, Angew. Chem. Int. Ed. 41 (2002) 2483–2487, https://doi.org/10.1002/1521-3773(20020715)41:14<2483::AID-ANIE2483>3.0.CO;2-U.

[78] G.A. Mazzocchin, M. Del Favero, G. Tasca, Analysis of pigments from Roman wall paintings found in the "Agro Centuriato" of Julia Concordia (Italy), Ann. Chim. 97 (9) (2007) 905–913, https://doi.org/10.1002/adic.200790075.

[79] T. Rehren, Ramesside glass-colouring crucibles, Archaeometry 39 (2) (1997) 355–368, https://doi.org/10.1111/j.1475-4754.1997.tb00812.x.

[80] A.A. Gambardella, M. Cotte, W. De Nolf, K. Schnetz, R. Erdmann, R. Van Elsas, V. Gonzalez, A. Wallert, P.D. Iedema, M. Eveno, K. Keune, Sulfur K-edge micro- and full-field XANES identify marker for preparation method of ultramarine pigment from lapis lazuli in historical paints, Sci. Adv. 6 (2020) eaay8782, https://doi.org/10.1126/sciadv.aay8782.

[81] M.B. Buscaglia, E.B. Halac, M. Reinoso, F. Marte, The palette of Pio Collivadino (1869–1945) throughout his career, J. Cult. Herit. 44 (2020) 27–37, https://doi.org/10.1016/j.culher.2020.02.012.

[82] J.S. Pozo-Antonio, T. Rivas, A. Dionísio, D. Barral, E.C. Cardell, Effect of a SO_2 rich atmosphere on tempera paint Mock-Ups. Part 1: accelerated aging of smalt and Lapis Lazuli-based paints, Minerals 10 (2020) 427–451, https://doi.org/10.3390/min10050427.

[83] R. Fontana, P. Baraldi, M.E. Fedi, M. Galeotti, S. Omarini, P. Zannini, J. Striova, Notes on Vestorius' Blue – New findings and investigations, J. Cult. Herit. 45 (2020) 370–378, https://doi.org/10.1016/j.culher.2020.03.002.

[84] A. Panagopoulou, K. Karanasios, G. Xanthopoulou, Ancient Egyptian Blue (CaCuSi4O10) Pigment by modern solution combustion synthesis method, Eurasian Chem.-Technol. J. 18 (1) (2016) 31-37. 10.18321/ectj390.

[85] R.S. Popelka-Filcoff, J.D. Robertson, M.D. Glascock, C. Descantes, Trace element characterisation of ochre from geological sources, J. Radioanal. Nucl. Chem. 272 (1) (2007) 17–27, https://doi.org/10.1007/s10967-006-6836-x.

[86] R.F. Rifkin, Processing ochre in the Middle Stone Age: testing the inference of prehistoric behaviours from actualistically derived experimental data, J. Anthropol. Archaeol. 31 (2) (2011) 174–176, https://doi.org/10.1016/j.jaa.2011.11.004.

[87] S. Sotiropoulou, V. Perdikatsis, K. Birtacha, C. Apostolaki, A. Devetzi, Physicochemical characterization and provenance of colouring materials from Akrotiri-Thera in relation to their archaeological context and application, Archaeol. Anthropol. Sci. 4 (2012) 263–275, https://doi.org/10.1007/s12520-012-0099-y.

[88] I.E. Sajó, J. Kovács, K.E. Fitzsimmons, V. Jáger, G. Lengye, B. Viola, S. Talamo, J. J. Hublin, Core-Shell processing of natural pigment: Upper Palaeolithic red ochre from Lovas, Hungary, Plos One 10 (7) (2015), e0131762, https://doi.org/10.1371/journal.pone.0131762.

[89] B.S. Eiselt, R. Popelka-Filcoff, J.A. Darling, M. Glascock, Hematite Sources and archaeological ochres from Hohokam and O'odham sites in central Arizona: an experiment in type identification and characterization, J. Archaeol. Sci. 38 (2011) 3019–3028, https://doi.org/10.1016/j.jas.2011.06.030.

[90] C.C. Kolb, Provenance Studies in Archaeology, in: C. Smith (Ed.), Encyclopedia of Global Archaeology, Springer, New York, NY, 2014, https://doi.org/10.1007/978-1-4419-0465-2_327.

[91] M.A. Rajabzadeh, S. Rasti, Investigation on mineralogy, geochemistry and fluid inclusions of the Goushti hydrothermal magnetite deposit, Fars Province, SW Iran: a comparison with IOCGs, Ore Geol. Revi. 82 (2017) 93–107, https://doi.org/10.1016/j.oregeorev.2016.11.025.

[92] A. Mücke, Chamosite, siderite and the environmental conditions of their formation in chamosite-type Phanerozoic ooidal ironstones, Ore Geol. Revi. 28 (2006) 235–249, https://doi.org/10.1016/j.oregeorev.2005.03.004.

[93] N. Attard Montalto, The characterisation and provenance of ancient ochres, Ph.D Cranfield Health, Cranfield University, 2010, p. 10. Available at: https://core.ac.uk/download/pdf/40025237.pdf.

[94] A.H. Rahiminejad, H. Zand-Moghada, Synsedimentary formation of ooidal ironstone: an example from the Jurassic deposits of SE central Iran, Ore Geol. Rev. 95 (2018) 238–257, https://doi.org/10.1016/j.oregeorev.2018.02.028.
[95] V. Vandeginste, C.M. John, Influence of climate and dolomite composition on dedolomitization: Insights from a multi-proxy study in the central Oman Mountains, J. Sediment. Res. 82 (3–4) (2012) 177–195, https://doi.org/10.2110/jsr.2012.19.
[96] I.S. Al-Aasm, F. Ghazban, M. Ranjbaran, Dolomitization and related fluid evolution in the Oligocene – Miocene Asmari Formation, Gachsaran area, SW Iran: Petrographic and isotopic evidence, J. Pet. Geol. 32 (3) (2009) 287–304, https://doi.org/10.1111/j.1747-5457.2009.00449.x.
[97] R.F. Beeston, H. Becker, Investigation of Ancient Roman Pigments by Portable X-ray Fluorescence Spectroscopy and Polarized Light Microscopy, in: R. A. Armitage, J.H. Burton, (Eds.), Archaeological Chemistry VIII. ACS Symposium Series, vol. 1147, American Chemical Society, Washington, DC, 2013, pp. 19-41. 10.1021/bk-2013-1147.ch002.
[98] M. Rudmin, I. Reva, E. Sokol, E. Abdullayev, A. Ruban, A. Kudryavtsev, O. Tolkachev, A. Mazurov, Minerals of rare earth elements in high-phosphorus Ooidal ironstones of the Western Siberia and Turgai Depression, Minerals 10 (1) (2019) 11, https://doi.org/10.3390/min10010011.
[99] A. Manasse, M. Mellini, Iron (hydr)oxide nanocrystals in raw and burnt sienna pigments, Eur. J. Mineral. 18 (6) (2006) 845–853, https://doi.org/10.1127/0935-1221/2006/0018-0845.
[100] F. D'Errico, R.M. Moreno, R.F. Rifkin, Technological, elemental and colorimetric analysis of an engraved ochre fragment from the Middle Stone Age levels of Klasies River Cave 1, South Africa, J. Archaeol. Sci. 39 (4) (2012) 942–952, https://doi.org/10.1016/j.jas.2011.10.032.
[101] I. Watts, The pigments from Pinnacle Point Cave 13B, Western Cape, South Africa, J. Hum. Evol. 59 (3–4) (2010) 392–411, https://doi.org/10.1016/j.jhevol.2010.07.006.
[102] S. Judson, Palaeolithic paint, Science 130 (3377) (1959) 708, https://doi.org/10.1126/science.130.3377.708.
[103] S. Hojati K. Hossein, Genesis and Distribution of Palygorskite in Iranian Soils and Sediments, in: E. Galàn, A. Singer (Eds.), Dev. Clay Sci. (3) 8, Elsevier, Amsterdam, 2011, pp. 205–218.
[104] P. Gholami Zadeh, M.H. Adabib, A. Sadeghib, Microfacies, geochemistry and sequence stratigraphy of the Sarvak Formation (Mid Cretaceous) in the Kuh-e Siah and Kuh-e Mond, Fars area, southern Iran, J. Afr. Earth Sci. 160 (2019), 103634, https://doi.org/10.1016/j.jafrearsci.2019.103634.
[105] F. Froment, A. Tournie, P. Colomban, Raman identification of natural red to yellow pigments: ochre and iron-containing ores, J. Raman Spectrosc. 39 (5) (2008) 560–568, https://doi.org/10.1002/jrs.1858.
[106] C. Bedford, D. Wayne Robinson, D. Gandy, Emigdiano Blues: the California indigenous pigment palette and an in situ analysis of an exotic colour, Open, Archaeol. 4 (2018) 152–172, https://doi.org/10.1515/opar-2018-0010.
[107] F.J. Weatherhead, A. Buckley, Artists' pigments from Amarna, in: B.J. Kemp (Ed.), Amarna Reports V, Egypt Exploration Society, London, 1984, pp. 202–239.
[108] S. Di Lernia, S. Bruni, I. Cislaghi, M. Cremaschi, Colour in context. Pigments and other coloured residues from the Early-Middle Holocene site of Takarkori (SW Libya), Archaeol. Anthropol. Sci. 8 (2015) 381–402, https://doi.org/10.1007/s12520-017-0482-9.
[109] W.A. Tiller, Dendrites: Understanding of this familiar phenomenon has led to the development of useful man-made materials, Science 146 (1964) 871–879. https://doi:10.1126/ science.146.3646.871.
[110] O. Oudbashi, A. Hasanpour, Microscopic study on some Iron Age bronze objects from Western Iran, Herit. Sci. 4 (2016) 8, https://doi.org/10.1186/s40494-016-0079-0.
[111] C.P. Thornton, The emergence of complex metallurgy on the Iranian plateau: escaping the levantine paradigm, J. World Prehist. 22 (2009) 301–327, https://doi.org/10.1007/s10963-009-9019-1.
[112] P. Callieri, A bronze trumpet from Persepolis, in: S. Gondet, E. Haerink (Eds.), L'Orient est son jardin: hommage à Remy Boucharlat, Acta Iranica 58, Peeters Publishers, Leuven, 2018, pp. 71–80.
[113] M.L. Amadori, G. Poldi, A note on the composition of the trumpet in the Persepolis Museum. Appendix of A bronze trumpet from Persepolis, in: S. Gondet, E. Haerink (Eds.), L'Orient est son jardin: hommage à Remy Boucharlat, Acta Iranica 58, Peeters Publishers, Leuven, 2018, pp. 78–79.
[114] M. Emami, Analysis of Some Copper Alloy Artefacts from New Excavations in Parsa (Persepolis), in: A. Askari Chaverdi, P. Callieri (Eds.), From Palace to Town. Science for Archaeology, vol. 4, BraDypUS, 2017, pp. 38-44. 10.12977/from_palace_to_town_4.
[115] B. Overlaet, Luristan bronzes I. The field research, Encyclopaedia Iranica online, https://www.iranicaonline.org/articles/luristan-bronzes-i-the-field-research-2016 (Accessed: 16 July, 2020).
[116] S. J. Fleming, V.C. Pigott, C.P. Swann, S.K. Nash, Bronze in Luristan: preliminary analytical evidence from copper/bronze artifacts excavated by the Belgian mission in Iran, Iran. Antiq. XL (2005) 35–64. https://doi:10.2143/IA.40.0.583199.